On the Crystal Structure of Colloidally Prepared Metastable Ag_2Se Nanocrystals

Bryce A. Tappan,[†,§] Bonan Zhu,[‡,§] Patrick Cottingham,[†,§] Matthew Mecklenburg,[#] David O. Scanlon,[‡||††] and Richard L. Brutchey[†,*]

[†] Department of Chemistry, University of Southern California, Los Angeles, CA 90089, United States

[‡] Department of Chemistry, University College London, London WC1H 0AJ, United Kingdom

[||] Thomas Young Centre, University College London, Gower Street, London WC1E 6BT, United Kingdom

[††] Diamond Light Source Ltd., Diamond House, Harwell Science and Innovation Campus, Didcot, Oxfordshire OX11 0DE, UK

[#] Core Center of Excellence in Nano Imaging, University of Southern California, Los Angeles, CA 90089, United States

KEYWORDS: Ag_2Se, nanocrystal, metastable, tetragonal, anti-$PbCl_2$-like, pair distribution function, density functional theory

ABSTRACT: Structural polymorphism is known for many bulk materials; however, on the nanoscale metastable polymorphs tend to form more readily than in the bulk, and with more structural variety. One such metastable polymorph observed for colloidal Ag_2Se nanocrystals has traditionally been referred to as the "tetragonal" phase of Ag_2Se. While there are reports on the chemistry and properties of this metastable polymorph, its crystal structure, and therefore electronic structure, has yet to be determined. We report that an anti-$PbCl_2$-like structure type (space group $P2_1/n$) accurately describes the powder X-ray diffraction and X-ray total scattering patterns of colloidal Ag_2Se nanocrystals prepared by several different methods. Density functional theory (DFT) calculations indicate that the anti-$PbCl_2$-like Ag_2Se polymorph is a dynamically stable, narrow-band gap semiconductor. DFT results reveal a dense theoretical Ag_2Se phase space with many low-energy polymorphs, which helps explain the large number of polymorphs reported in the literature.

Polymorphism, or the ability of fixed compositions of matter to crystallize in two or more different crystal structures, is common in solid-state chemistry. The stability of different polymorphs is determined by their relative free energies under a given set of conditions (temperature, pressure, etc.).[1] While thermodynamics determine the relative free energies of polymorphs,[2] the kinetics of phase transitions dictate the time scales of the conversion of higher energy polymorphs to more stable polymorphs for a given set of conditions. Thus, if the activation energy of a phase transition is sufficiently large, it is possible for a polymorph to be observed far from the conditions where it is thermodynamically preferred, making it kinetically trapped or 'metastable.'

The increased surface energy and decreased lattice energy of nanocrystals leads to reduced activation energies for solid-solid phase transitions in nanocrystals relative to the same transitions in their bulk material analogs.[3–5] These differences enable the syntheses of certain nanocrystal phases at much lower temperatures than the analogous syntheses of bulk crystals. Additionally, differences in free energy between polymorphs change due to, in large part, the role of surface energy in determining thermodynamic stabilities of nanocrystals.[6–10]

Surface energetics play such a large role that they can favor the formation of polymorphs that are not observed in the corresponding bulk materials;[10–12] this phenomenon has been observed in the binary chalcogenide Ag_2Se. In the bulk, Ag_2Se crystallizes with an orthorhombic crystal structure ($P2_12_12_1$ space group) at temperatures up to ~133 °C (1 atm), at which point it undergoes a phase transition to a body-centered cubic structure ($Im\overline{3}m$ space group), which is stable until the melt at 897 °C.[13,14] While the orthorhombic and cubic phases are also observed on the nanoscale, other distinct polymorphs have been observed within colloidal Ag_2Se nanocrystals and thin films with sub-micron thicknesses.[15–20] Günter and Keusch tabulated a number of findings of Ag_2Se in unknown crystal structures;[15] they proposed a monoclinic, "pseudo-tetragonal" unit cell with $P2$ space group symmetry to describe the crystal structure of nanometer-thickness thin films of Ag_2Se. Since this report, numerous papers have referenced Günter and Keusch's "pseudo-tetragonal" unit cell when assigning a phase to metastable colloidal Ag_2Se nanocrystals that, by powder X-ray diffraction (XRD), appear to adopt a crystal structure distinct from both the known orthorhombic and cubic phases of Ag_2Se.[12,16,21–27] Most of these publications use the crystal system established by Günter and Keusch; that is, they refer to the metastable Ag_2Se nanocrystals as having a "pseudo-tetragonal" or "tetragonal" unit cell. However, there are no prior refinements of powder XRD data of these metastable Ag_2Se nanocrystals to the unit cell described by Günter and Keusch. Rather, the diffraction data has only been qualitatively compared to the *d*-spacings and lattice parameters reported by Günter and Keusch.[12,15,16,24]

This is perhaps unsurprising, as solving the crystal structure for a colloidal nanocrystal is quite difficult – single crystal structure determination is rare and Scherrer broadening complicates the analysis of powder diffraction data collected on nanocrystals with low-symmetry crystal structures in which reflections tend to overlap. Additionally, in the case of metastable Ag_2Se nanocrystals, attaining phase-pure samples can be difficult, as orthorhombic Ag_2Se easily forms along with the metastable phase, and/or the metastable phase can undergo some degree of phase relaxation to the orthorhombic polymorph after synthesis.[16,22] That said, structural knowledge of nanocrystals is critically important, as different polymorphs possess unique properties.[28] In the case of Ag_2Se, substantial changes in physical properties accompany solid-solid phase transitions.[29] For example, the orthorhombic phase of Ag_2Se is known to be a narrow-band gap semiconductor in the bulk (E_g = 0.15 eV), and orthorhombic Ag_2Se nanocrystals are promising for near-infrared detection and imaging applications and as topological insulators.[30–33] In contrast, the high-temperature cubic phase is electrically and ionically conductive, with highly mobile Ag^+ cations that move through a rigid body-centered Se^{2-} sub-lattice.[23,34,35] These properties of cubic Ag_2Se are desirable for solid-state electrolytes,[29,36,37] and the differences in electrical and thermal conductivity between orthorhombic and cubic Ag_2Se have been used to optimize thermoelectric responses at temperatures near the boundary of the orthorhombic-to-cubic phase transition.[38] Significantly less is known about "tetragonal" phase of Ag_2Se nanocrystals, in part because the crystal structure remains unresolved. However, Sahu et al. determined that the infrared absorption of metastable "tetragonal" Ag_2Se nanocrystals is broadly tunable through the near to mid-infrared region as a result of size-dependent quantum confinement.[21] Furthermore, it has been shown that the phase transitions of "tetragonal" Ag_2Se nanocrystals are dependent on the identity of the surface ligands bound to the colloidal Ag_2Se nanocrystals.[10,16,22,39,40]

Given that the crystal structure determines material properties, obtaining the structure solution to the unresolved metastable phase of Ag_2Se nanocrystals is crucial to advance our understanding of its optoelectronic properties. Herein, we find that the metastable phase of Ag_2Se, previously assigned as "tetragonal," is actually isostructural with the anti-$PbCl_2$-like structure type adopted by Ag_2S at ambient temperature and pressure, which crystallizes in the monoclinic space group $P2_1/n$.[41] Thus, previous assignments of the "tetragonal" unit cell are incorrect in the context of describing the crystal structure of colloidal metastable Ag_2Se nanocrystals. Density functional theory (DFT) calculations reveal that this anti-$PbCl_2$-like Ag_2Se is dynamically stable and is predicted to be a narrow-band gap semiconductor, consistent with experiments.

Nanocrystal Preparation

Colloidal Ag_2Se nanocrystals in the metastable "tetragonal" phase were prepared by the method of Wang et al.[16] In brief, the nanocrystals were prepared via solvothermal synthesis in DMF by combining $AgNO_3$, SeO_2, oleic acid, and polyvinyl pyrrolidone (PVP) and heating to 200 °C for 9-12 h. This solvothermal method was chosen because the resulting PVP-capped Ag_2Se nanocrystals persist in the metastable "tetragonal" phase longer (i.e., days), and produce larger nanocrystals to minimize Scherrer broadening, than other preparative methods.[16,22,26]

Transmission electron microscopy (TEM) and energy dispersive X-ray spectroscopy (EDX) elemental mapping reveal that the resulting Ag_2Se nanocrystals are consistent with those previously reported for the PVP-enabled solvothermal method (**Figure S1**).[16] TEM images of the Ag_2Se nanocrystals show that the nanocrystals are fairly large, with an average diameter of 143 ± 33 nm ($\sigma/\bar{d}$ = 23%, **Figure S1a**). Elemental analysis was performed using TEM-EDX, the results of which show that Ag and Se are distributed evenly throughout the particles and that the nanocrystals are close to the ideal stoichiometry, with an average composition of $Ag_{2.1}Se_{1.0}$ (**Figure S1c,d**).

Structure Determination

Laboratory powder XRD data collected on the Ag_2Se nanocrystals are provided in **Figure 1a**, and are in qualitative agreement with prior reports of this metastable phase.[16,22,40] This data was obtained immediately after the nanocrystal synthesis. A simulated powder XRD pattern of the theoretical "tetragonal" structure reported by Günter and Keusch is shown in red. While there are a few peaks in the XRD pattern that correspond to reflections in the simulated "tetragonal" pattern, it is clear that the "tetragonal" pattern does not account for most of the experimentally observed reflections. All attempts to perform Rietveld refinements of the "tetragonal" structure against the experimental XRD data diverged to unphysical values. Alternatively, a Rietveld refinement with a good quality-of-fit was obtained starting with the structure type of a closely related material; namely, anti-$PbCl_2$-like Ag_2S,[41] which is shown in blue (**Figure 1a**). This structure accounts for nearly all reflections in the powder XRD pattern of the Ag_2Se nanocrystals, although a small phase fraction (weight fraction < 1%) of the orthorhombic $P2_12_12_1$ Ag_2Se structure accounts for some residual low-intensity reflections. For this two-phase refinement, a Rw of 4.32% was achieved. Refined values of the anti-$PbCl_2$-like Ag_2Se phase (a = 4.2960(8) Å; b = 6.9982(6) Å; c = 8.1977(27) Å; β = 101.278(7)°) are given in **Table S1**. The anti-$PbCl_2$-like structure also provided satisfactory refinements to powder XRD data collected on nanocrystals prepared by alternate oleylamine- and *N*-heterocyclic carbene-enabled syntheses,[16,26] as shown in **Figures S2,3**. In addition, high resolution TEM images of the PVP-capped Ag_2Se nanocrystals reveal that lattice fringes visible near the edges of the particles have measured *d*-spacings of 0.37 nm, corresponding to the (110) lattice planes of the anti-$PbCl_2$ structure (**Figure S1b**). Thus, it appears that the average structure of the metastable Ag_2Se nanocrystals can be adequately described as anti-$PbCl_2$-like.

The anti-$PbCl_2$-like structure is monoclinic with space group $P2_1/n$. Whereas the "tetragonal" structure of Ag_2Se shown in **Figure 1b** is a slightly distorted face-centered cubic-lattice of Se^{2-} anions containing interstitial Ag^+ cations, the anti-$PbCl_2$-like structure shown in **Figure 1c** features distorted edge-sharing $AgSe_4$ tetrahedra. The observation of the anti-$PbCl_2$-like structure of Ag_2S in Ag_2Se nanocrystals is consistent with other reports of metal selenide nanocrystals that adopt metastable crystal structures not found in the bulk, but are isostructural with known polymorphs that form in the bulk for analogous metal sulfides.[10,42] In the text below, the phase previously referred to as "tetragonal" will now be referred to as anti-$PbCl_2$-like.

Given the limitations of diffraction studies on colloidal nanocrystals, a dual-space approach that combines Rietveld and pair distribution function (PDF) analysis of X-ray total scattering data is often useful.[43–45] The PDF is a histogram of atom-atom distances that represent the local atomic (Å-scale) structure of a material. The PDFs given in **Figure 2** were extracted from variable temperature synchrotron X-ray total scattering data collected on the same sample of Ag_2Se nanocrystals at T = 25 °C, 120 °C, and then cooled to 25 °C again. Crystallographic parameters of the phases in each of the PDF fits are given in **Table S2.** While the maximum temperature T = 120 °C is below the temperature of the orthorhombic-to-cubic phase transition in the bulk, it is above the "pseudo-tetragonal"-to-cubic phase transition for the Ag_2Se nanocrystals prepared by the PVP-enabled solvothermal method, as reported by Sahu et al.[22] Due

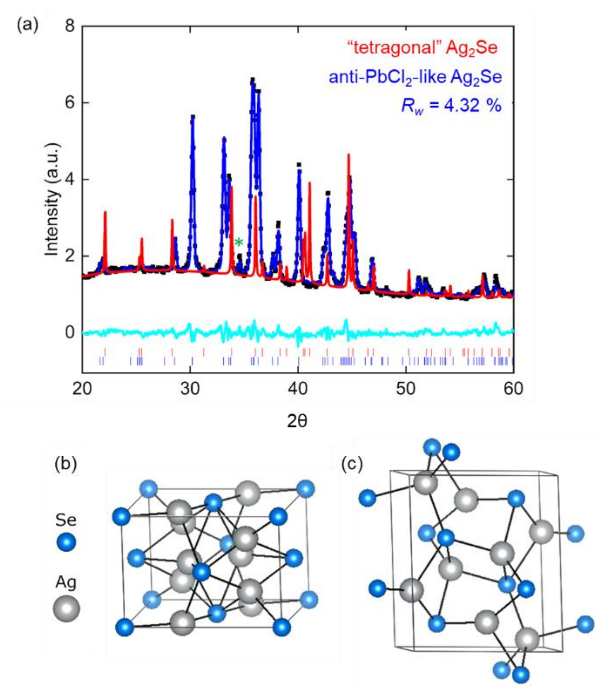

Figure 1. (a) Rietveld refinement of the proposed anti-$PbCl_2$-like structure to the experimental powder XRD pattern of metastable Ag_2Se nanocrystals (λ = 1.5406 Å). The experimental diffraction pattern is shown with black data points, and the refined model is shown as the blue trace, with the difference pattern shown below in turquoise. For reference, the calculated powder diffraction pattern of Günter and Keusch's "tetragonal" phase is shown in red. The most prominent peak arising from orthorhombic Ag_2Se is marked by a green asterisk (*), which forms from spontaneous relaxation of the anti-$PbCl_2$-like phase. (b) Unit cell of Günter and Keusch's "tetragonal" phase.[15] (c) Unit cell of the proposed anti-$PbCl_2$-like polymorph of Ag_2Se.

to the 2:1 atomic ratio of Ag to Se, and the relative X-ray atomic scattering factor (Z) of Ag relative to Se, the Ag-Ag interatomic distances contribute the most intensity to the PDF, followed by Ag-Se distances and, finally, Se-Se distances.

The differences between the PDFs for T = 25 and 120 °C are readily apparent. In particular, distinct features at $G(r)$ = 9.7, 12.1, and 13.5 Å that are clearly present at 25 °C are not apparent at 120 °C. This loss of features is consistent with a phase transition from a lower-symmetry to a higher-symmetry crystal structure. The high-temperature cubic structure features highly mobile Ag^+ cations, which are expected to generate broadened features corresponding to Ag-Ag and Ag-Se distances in the PDF of Ag_2Se. A very good fit to the PDF of the initial measurement at T = 25 °C was obtained using a model in which the majority phase fraction was anti-$PbCl_2$-like Ag_2Se. The best fit to the data, shown in **Figure 2a**, occurred when a fraction of orthorhombic Ag_2Se and a small fraction of elemental Se were included. The relative phase fractions in the model for anti-$PbCl_2$-like Ag_2Se, orthorhombic Ag_2Se, and elemental Se were 81.2%, 15.9%, and 2.9%, respectively. The presence of some orthorhombic Ag_2Se is expected and consistent with reports that metastable PVP-capped Ag_2Se nanocrystals relax to the orthorhombic structure at room temperature on a timescale of days to

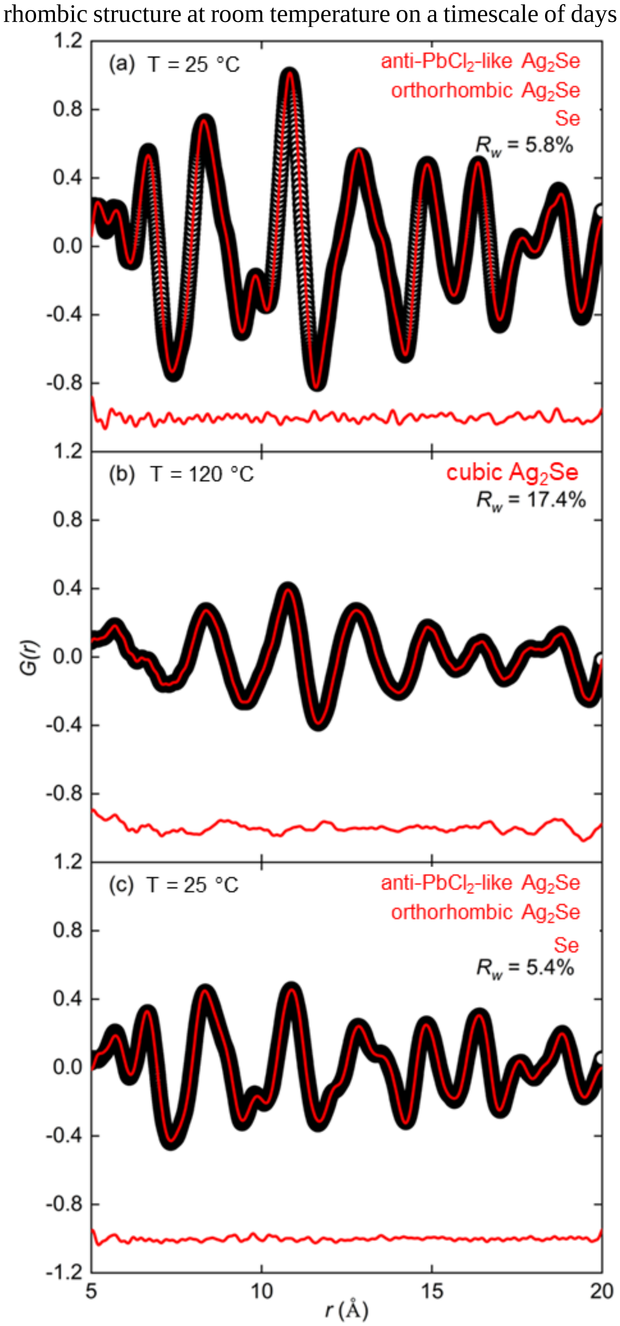

Figure 2. PDFs extracted from variable temperature synchrotron X-ray total scattering data collected at (a) 25 °C, (b) 120 °C, and (c) again at 25 °C (λ = 0.143 Å). Black circles indicate the PDF and upper red lines indicate the fit. Lower red lines indicate the difference between the data and the fit.

weeks; given the ~1 week between the synthesis and the analysis of Ag_2Se nanocrystals on the beamline, partial relaxation of the anti-$PbCl_2$-like phase was therefore inevitable and expected. The small phase fraction of elemental Se is likely left over from reduced SeO_2 precursor in the solvothermal synthesis. The statistical quality-of-fit for this three-phase model is R_w = 5.8%.

The PDF for the nanocrystals at T = 120 °C, shown in **Figure 2b**, is well-described by the high-temperature cubic structure of Ag_2Se, with R_w = 17.4%. The cubic Ag_2Se structure contains three crystallographically distinct Ag sites, each of which is partially occupied. Allowing each of these occupancies to refine freely led to a Ag/Se ratio of 1.78:1. This apparently Ag-deficient stoichiometry is likely due to some of the Ag^+ ions in

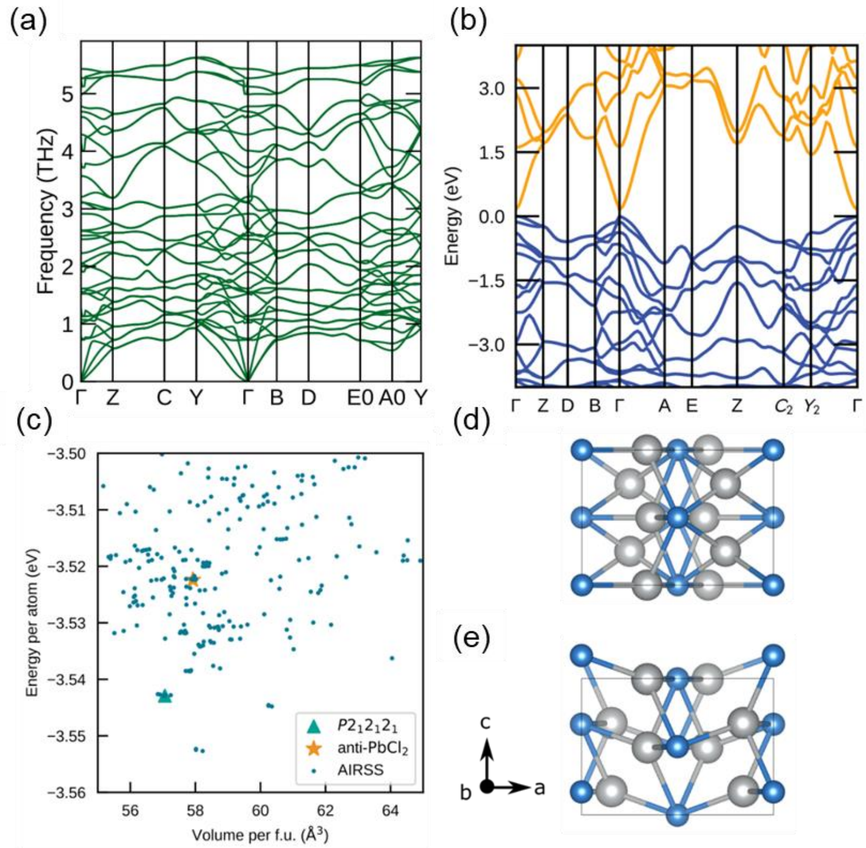

Figure 3. (a) The phonon band structure of the anti-$PbCl_2$-like Ag_2Se phase showing that it is dynamically stable. (b) The electronic band structure of the anti-$PbCl_2$-like phase computed using the HSE06 hybrid functional[46] showing that it is a narrow band gap semiconductor. (c) The total energy plotted against the volume per formula unit for structures obtained through searching (AIRSS) as well as the orthorhombic $P2_12_12_1$ (▲) and the anti-$PbCl_2$-like $P2_1/n$ (★) phases. The PBEsol exchange-correlation functional is used here. (d) The $P2$ unit cell reported by Günter and Keusch. (e) The unit cell in (d) optimized using DFT with the PBEsol functional. Significant structural changes take place – the adjacent [200] planes shear in the [001] direction, and the Ag atoms move to different sites.

the ionically conducting cubic Ag_2Se phase being broadly distributed between crystallographic sites and not populating any distinct atom-atom distances. When a phase fraction of elemental Se was included in these fits, the phase fraction refined towards a negligibly small value.

Figure 2c shows the PDF of the same PVP-capped Ag_2Se nanocrystals after they were returned to room temperature. Once again, the three-phase model with anti-$PbCl_2$-like Ag_2Se, orthorhombic Ag_2Se, and elemental Se provides a close description of the PDF with R_w = 5.4%. For this PDF, the fraction of the orthorhombic phase increased to 41.8% and the elemental Se fraction increased to 4.7%. There are several plausible explanations for this; it is possible that particle sintering during heating of our sample converted nanocrystals in anti-$PbCl_2$-like structure into larger particles, for which the anti-$PbCl_2$-like structure is highly unstable.[22] Furthermore, the initial 15% phase fraction of orthorhombic Ag_2Se may facilitate conversion of anti-$PbCl_2$-like nanocrystals to the orthorhombic phase within a heating/cooling cycle. Indeed, the rate of polymorphic phase transitions in powders is nucleation-limited, and is proportional to the number of potential nuclei present within a sample at a given temperature.[28] Since the orthorhombic phase comprised 15% of the Ag_2Se sample prior to a heating/cooling cycle, these crystallites may have served as nucleation and growth sites for a larger fraction of orthorhombic Ag_2Se upon cooling.

Concurrent with the collection of synchrotron X-ray total scattering data, synchrotron powder XRD data were also collected on the same samples at each temperature. Rietveld refinements were performed to those data and the results are shown in **Figure S4** and refined crystallographic parameters are reported in **Table S3.** In these refinements a good quality-of-fit was obtained with the same combinations of phases at each temperature as in the PDF fits, suggesting good agreement between the local and average structures.

Density Functional Theory

The phase space of Ag_2Se was explored computationally using ab-initio random structure searching (AIRSS). In addition to the experimental orthorhombic $P2_12_12_1$ phase, a large number of other polymorphs emerged (**Figure 3c**). This crowded Ag_2Se energy landscape is consistent with the experimental observations of a complex phase space on the nanoscale.[15]

Intriguingly, the DFT calculations suggest the existence of Ag_2Se structures with lower energies than the empirically stable, low-temperature orthorhombic phase. Notably, the energetics among different phases appear to depend on the exchange-correlation functionals. In particular, the PBE exchange-correlation functional, which often overestimates the lattice constant of solids, biases towards structures that are less dense (e.g., those with large volumes per formula unit). On the other hand, the PBEsol functional appears to give more reliable energy rankings, although there are still two phases predicted to be more stable than the orthorhombic $P2_12_12_1$ phase. It is possible that the orthorhombic $P2_12_12_1$ phase is not predicted to be the most energetically stable structure due to the neglect of entropic stabilization in our calculations.

The anti-$PbCl_2$-like phase was also found through ab-initio random structure searching when limiting the possible polymorphs of Ag_2Se to the $P2_1/n$ space group. Here, the anti-$PbCl_2$-like phase was ~20 meV/atom higher than the orthorhombic polymorph using the PBEsol functional, and many other theoretical polymorphs were predicted to lie between these two phases. We recomputed the energies of selected low-energy phases using the LDA and PBE functionals, as well as the hybrid functional HSE06. The anti-$PbCl_2$-like phase is found to be consistently higher in energy than the stable orthorhombic polymorph, although the difference varies between 5 meV/atom and 25 meV/atom, as shown in **Figure S5**.

The calculated electronic structure of the anti-$PbCl_2$-like phase shows that it is a semiconductor with a narrow gap ~0.13 eV at the Γ-point, as shown in **Figure 3b**. We found that the orthorhombic polymorph also has a narrow gap, at ~0.05 eV, consistent with previous DFT work.[47] The band gap openings only take place with HSE06 function, as both polymorphs have no band gap if the PBEsol functional is used instead. These band gaps are quite close to experimentally determined optical band gap measurements for these two polymorphs of Ag_2Se.[21,48] Finite-displacement phonon calculations indicate that the anti-$PbCl_2$-like phase is dynamically stable, and no imaginary frequencies are observed **Figure 3a**.

Interestingly, the $P2$ unit cell reported by Günter and Keusch appears to be far from a local minimum on the potential energy surface; significant structural rearrangements occur during geometry relaxation calculations (**Figure 3d,e**), and the relaxed structure is still ~20 meV/atom higher in energy than the anti-$PbCl_2$-like phase. Although the instability of Günter and Keusch's $P2$ phase means that it is unlikely to exist in a bulk form, strain involved in thin films could play an important role for stabilization of this polymorph, but it cannot be sustained with increasing thickness.

To conclude, we have shown that the metastable polymorph of colloidal Ag_2Se nanocrystals, commonly referred to as the "tetragonal" phase, more accurately adopts an anti-$PbCl_2$-like structure. DFT calculations reveal that this polymorph is a true local minimum within the energy-structure landscape of Ag_2Se. Electronic structure calculations indicate that anti-$PbCl_2$-like Ag_2Se is a narrow-band gap semiconductor. In addition, we find that this phase space is crowded with theoretical, relatively low-energy polymorphs, which may explain the preponderance of reports of different Ag_2Se polymorphs on the nanoscale.

ASSOCIATED CONTENT

Supporting Information.

The Supporting Information is available free of charge on the ACS Publications website.

Synthesis and characterization details, additional Rietveld analyses, TEM and TEM-EDS data, additional PDF data, DFT results (PDF)

AUTHOR INFORMATION

Corresponding Author

*E-mail: brutchey@usc.edu.
ORCID
Richard L. Brutchey: 0000-0002-7781-5596

Author Contributions

§B.A.T., B.Z., and P.C. contributed equally to this work.

ACKNOWLEDGMENT

The experimental work was supported by the U.S. Department of Energy, Office of Science, Office of Basic Energy Sciences, under Grant No. DE-FG02-11ER46826 to R.L.B. Use of the Advanced Photon Source at Argonne National Laboratory was supported by the U.S. Department of Energy, Office of Science, Office of Basic Energy Sciences, under Contract No. DE-AC02-06CH11357. Via our membership of the UK's HEC Materials Chemistry Consortium, which is funded by the UK Engineering and Physical Sciences Research Council (EPSRC; EP/L000202, EP/R029431, EP/T022213), this work used the ARCHER and ARCHER2 UK National Supercomputing Services. We are also grateful to the UK Materials and Molecular Modelling Hub (MMM Hub), which is partially funded by the EPSRC (EP/P020194, EP/T022213), for computational resources on the Thomas and Young supercomputers, and to UCL for access to the Legion (Legion@UCL), Myriad (Myriad@UCL) and Kathleen (Kathleen@UCL) supercomputers.

REFERENCES

(1) Parija, A.; Waetzig, G. R.; Andrews, J. L.; Banerjee, S. Traversing Energy Landscapes Away from Equilibrium: Strategies for Accessing and Utilizing Metastable Phase Space. *J. Phys. Chem. C* **2018**, *122* (45), 25709–25728. https://doi.org/10.1021/acs.jpcc.8b04622.

(2) Sun, W.; Dacek, S. T.; Ong, S. P.; Hautier, G.; Jain, A.; Richards, W. D.; Gamst, A. C.; Persson, K. A.; Ceder, G. The Thermodynamic Scale of Inorganic Crystalline Metastability. *Sci. Adv.* **2016**, *2* (11), e1600225. https://doi.org/10.1126/sciadv.1600225.

(3) Son, D. H.; Hughes, S. M.; Yin, Y.; Alivisatos, A. P. Cation Exchange Reactions in Ionic Nanocrystals. *Science* **2004**, *306* (5698), 1009–1012. https://doi.org/10.1126/science.1103755.

(4) Trizio, L. D.; Manna, L. Forging Colloidal Nanostructures via Cation Exchange Reactions https://pubs.acs.org/doi/abs/10.1021/acs.chemrev.5b00739 (accessed Mar 23, 2018).

(5) Beberwyck, B. J.; Surendranath, Y.; Alivisatos, A. P. Cation Exchange: A Versatile Tool for Nanomaterials Synthesis. *J. Phys. Chem. C* **2013**, *117* (39), 19759–19770. https://doi.org/10.1021/jp405989z.

(6) McHale, J. M.; Auroux, A.; Perrotta, A. J.; Navrotsky, A. Surface Energies and Thermodynamic Phase Stability in Nanocrystalline Aluminas. *Science* **1997**, *277* (5327), 788–791. https://doi.org/10.1126/science.277.5327.788.

(7) Lu, H. M.; Jiang, Q. Size-Dependent Surface Energies of Nanocrystals. *J. Phys. Chem. B* **2004**, *108* (18), 5617–5619. https://doi.org/10.1021/jp0366264.

(8) Cozzoli, P. D.; Manna, L.; Curri, M. L.; Kudera, S.; Giannini, C.; Striccoli, M.; Agostiano, A. Shape and Phase Control of Colloidal ZnSe Nanocrystals. *Chem. Mater.* **2005**, *17* (6), 1296–1306. https://doi.org/10.1021/cm047874v.

(9) Janssen, A.; Nguyen, Q. N.; Xia, Y. Colloidal Metal Nanocrystals with Metastable Crystal Structures. *Angew. Chem. Int. Ed.* *n/a* (n/a). https://doi.org/https://doi.org/10.1002/anie.202017076.

(10) Tappan, B. A.; Brutchey, R. L. Polymorphic Metastability in Colloidal Semiconductor Nanocrystals. *ChemNanoMat* **2020**, *6* (11), 1567–1588. https://doi.org/https://doi.org/10.1002/cnma.202000406.

(11) Soriano, R. B.; Arachchige, I. U.; Malliakas, C. D.; Wu, J.; Kanatzidis, M. G. Nanoscale Stabilization of New Phases in the PbTe–Sb2Te3 System: PbmSb2nTem+3n Nanocrystals. *J. Am. Chem. Soc.* **2013**, *135* (2), 768–774. https://doi.org/10.1021/ja309626q.

(12) Sahu, A.; Qi, L.; Kang, M. S.; Deng, D.; Norris, D. J. Facile Synthesis of Silver Chalcogenide (Ag2E; E = Se, S, Te) Semiconductor Nanocrystals. *J. Am. Chem. Soc.* **2011**, *133* (17), 6509–6512. https://doi.org/10.1021/ja200012e.

(13) Karakaya, I.; Thompson, W. T. The Ag-Se (Silver-Selenium) System. *Bull. Alloy Phase Diagr.* **1990**, *11* (3), 266. https://doi.org/10.1007/BF03029297.

(14) Olekseyuk, I. D.; Krykhovets, O. V. The Ag2Se–In2Se3–SnSe2 System. *J. Alloys Compd.* **2001**, *316* (1), 193–202. https://doi.org/10.1016/S0925-8388(00)01283-4.

(15) Günter, J. R.; Keusch, P. Thickness Dependence of Structure in Thin Films of Low-Temperature Silver Selenide. *Ultramicroscopy* **1993**, *49* (1), 293–307. https://doi.org/10.1016/0304-3991(93)90236-Q.

(16) Wang, J.; Fan, W.; Yang, J.; Da, Z.; Yang, X.; Chen, K.; Yu, H.; Cheng, X. Tetragonal–Orthorhombic–Cubic Phase Transitions in Ag2Se Nanocrystals. *Chem. Mater.* **2014**, *26* (19), 5647–5653. https://doi.org/10.1021/cm502317g.

(17) Gates, B.; Mayers, B.; Wu, Y.; Sun, Y.; Cattle, B.; Yang, P.; Xia, Y. Synthesis and Characterization of Crystalline Ag2Se Nanowires Through a Template-Engaged Reaction at Room Temperature. *Adv. Funct. Mater.* **2002**, *12* (10), 679–686. https://doi.org/https://doi.org/10.1002/1616-3028(20021016)12:10<679::AID-ADFM679>3.0.CO;2-#.

(18) Abdullayev, A. G.; Shafizade, R. B.; Krupnikov, E. S.; Kiriluk, K. V. Phase Formation and Kinetics of the Phase Transition in Ag2Se Thin Films. *Thin Solid Films* **1983**, *106* (3), 175–184. https://doi.org/10.1016/0040-6090(83)90479-0.

(19) Saito, Y.; Sato, M.; Shiojiri, M. Orientation in Ag2Se Polymorphic Films Produced by the Reaction of Silver Films with Selenium. *Thin Solid Films* **1981**, *79* (3), 257–266. https://doi.org/10.1016/0040-6090(81)90314-X.

(20) Asadov, Y. G.; Aliyev, Y. I.; Babaev, A. G. Polymorphic Transformations in Cu2Se, Ag2Se, AgCuSe and the Role of Partial Cation-Cation and Anion-Anion Replacement in Stabilizing Their Modifications. *Phys. Part. Nucl.* **2015**, *46* (3), 452–474. https://doi.org/10.1134/S106377961503003X.

(21) Sahu, A.; Khare, A.; Deng, D. D.; Norris, D. J. Quantum Confinement in Silver Selenide Semiconductor Nanocrystals. *Chem. Commun.* **2012**, *48* (44), 5458–5460. https://doi.org/10.1039/C2CC30539A.

(22) Sahu, A.; Braga, D.; Waser, O.; Kang, M. S.; Deng, D.; Norris, D. J. Solid-Phase Flexibility in Ag2Se Semiconductor Nanocrystals. *Nano Lett.* **2014**, *14* (1), 115–121. https://doi.org/10.1021/nl4041498.

(23) Chen, N.; R. Scimeca, M.; J. Paul, S.; B. Hafiz, S.; Yang, Z.; Liu, X.; Yang, F.; Ko, D.-K.; Sahu, A. High-Performance Thermoelectric Silver Selenide Thin Films Cation Exchanged from a Copper Selenide Template. *Nanoscale Adv.* **2020**, *2* (1), 368–376. https://doi.org/10.1039/C9NA00605B.

(24) Tan, L.; Fu, J.; Liu, S. Growth of Photoluminescent Ag2Se Nanowires from a Simple Precursor Solution. *CrystEngComm* **2014**, *16* (46), 10534–10538. https://doi.org/10.1039/C4CE01294A.

(25) Qu, J.; Goubet, N.; Livache, C.; Martinez, B.; Amelot, D.; Gréboval, C.; Chu, A.; Ramade, J.; Cruguel, H.; Ithurria, S.; Silly, M. G.; Lhuillier, E. Intraband Mid-Infrared Transitions in Ag2Se Nanocrystals: Potential and Limitations for Hg-Free Low-Cost Photodetection. *J. Phys. Chem. C* **2018**, *122* (31), 18161–18167. https://doi.org/10.1021/acs.jpcc.8b05699.

(26) Lu, H.; Brutchey, R. L. Tunable Room-Temperature Synthesis of Coinage Metal Chalcogenide Nanocrystals from N-Heterocyclic Carbene Synthons. *Chem. Mater.* **2017**, *29* (3), 1396–1403. https://doi.org/10.1021/acs.chemmater.6b05293.

(27) Tappan, B. A.; Horton, M. K.; Brutchey, R. L. Ligand-Mediated Phase Control in Colloidal AgInSe2 Nanocrystals. *Chem. Mater.* **2020**, *32* (7), 2935–2945. https://doi.org/10.1021/acs.chemmater.9b05163.

(28) Anwar, J.; Zahn, D. Polymorphic Phase Transitions: Macroscopic Theory and Molecular Simulation. *Adv. Drug Deliv. Rev.* **2017**, *117*, 47–70. https://doi.org/10.1016/j.addr.2017.09.017.

(29) Ayele, D. W. A Facile One-Pot Synthesis and Characterization of Ag2Se Nanoparticles at Low Temperature. *Egypt. J. Basic Appl. Sci.* **2016**, *3* (2), 149–154. https://doi.org/10.1016/j.ejbas.2016.01.002.

(30) Zhu, C.-N.; Jiang, P.; Zhang, Z.-L.; Zhu, D.-L.; Tian, Z.-Q.; Pang, D.-W. Ag2Se Quantum Dots with Tunable Emission in the Second Near-Infrared Window. *ACS Appl. Mater. Interfaces* **2013**, *5* (4), 1186–1189. https://doi.org/10.1021/am303110x.

(31) Kim, J.; Hwang, A.; Lee, S.-H.; Jhi, S.-H.; Lee, S.; Park, Y. C.; Kim, S.; Kim, H.-S.; Doh, Y.-J.; Kim, J.; Kim, B. Quantum Electronic Transport of Topological Surface States in β-Ag2Se Nanowire. *ACS Nano* **2016**, *10* (4), 3936–3943. https://doi.org/10.1021/acsnano.5b07368.

(32) Graddage, N.; Ouyang, J.; Lu, J.; Chu, T.-Y.; Zhang, Y.; Li, Z.; Wu, X.; Malenfant, P. R. L.; Tao, Y. Near-Infrared-II Photodetectors Based on Silver Selenide Quantum Dots on Mesoporous TiO2 Scaffolds. *ACS Appl. Nano Mater.* **2020**, *3* (12), 12209–12217. https://doi.org/10.1021/acsanm.0c02686.

(33) Yang, X.; Wang, C.; Zhang, X.; Wang, Y.; Gao, F.; Sun, L.; Xu, W.; Qiao, C.; Zhang, G. Photothermal and Adsorption Effects of Silver Selenide Nanoparticles Modified by Different Surfactants in Nursing Care of Cancer Patients. *Sci. Technol. Adv. Mater.* **2020**, *21* (1), 584–592. https://doi.org/10.1080/14686996.2020.1800367.

(34) Usuki, T.; Abe, K.; Uemura, O.; Kameda, Y. Ionic Conduction in Liquid Ag–Se and Ag–Te Systems. *J. Phys. Soc. Jpn.* **2001**, *70* (7), 2061–2067. https://doi.org/10.1143/JPSJ.70.2061.
(35) Jood, P.; Chetty, R.; Ohta, M. Structural Stability Enables High Thermoelectric Performance in Room Temperature Ag2Se. *J. Mater. Chem. A* **2020**, *8* (26), 13024–13037. https://doi.org/10.1039/D0TA02614J.
(36) Jang, J.; Pan, F.; Braam, K.; Subramanian, V. Resistance Switching Characteristics of Solid Electrolyte Chalcogenide Ag2Se Nanoparticles for Flexible Nonvolatile Memory Applications. *Adv. Mater.* **2012**, *24* (26), 3573–3576. https://doi.org/10.1002/adma.201200671.
(37) Boolchand, P.; Bresser, W. J. Mobile Silver Ions and Glass Formation in Solid Electrolytes. *Nature* **2001**, *410* (6832), 1070–1073. https://doi.org/10.1038/35074049.
(38) Xiao, C.; Xu, J.; Li, K.; Feng, J.; Yang, J.; Xie, Y. Superionic Phase Transition in Silver Chalcogenide Nanocrystals Realizing Optimized Thermoelectric Performance. *J. Am. Chem. Soc.* **2012**, *134* (9), 4287–4293. https://doi.org/10.1021/ja2104476.
(39) Wang, J. L.; Feng, H.; Fan, W. L. Solvothermal Preparation and Thermal Phase Change Behaviors of Nanosized Tetragonal-Phase Silver Selenide (Ag2Se) /AMR.850-851.128 (accessed May 26, 2020).
(40) Wang, J.; Chen, K.; Gong, M.; Xu, B.; Yang, Q. Solution–Solid–Solid Mechanism: Superionic Conductors Catalyze Nanowire Growth. *Nano Lett.* **2013**, *13* (9), 3996–4000. https://doi.org/10.1021/nl400637w.
(41) Santamaría-Pérez, D.; Marqués, M.; Chuliá-Jordán, R.; Menendez, J. M.; Gomis, O.; Ruiz-Fuertes, J.; Sans, J. A.; Errandonea, D.; Recio, J. M. Compression of Silver Sulfide: X-Ray Diffraction Measurements and Total-Energy Calculations. *Inorg. Chem.* **2012**, *51* (9), 5289–5298. https://doi.org/10.1021/ic300236p.
(42) Ng, M. T.; Boothroyd, C. B.; Vittal, J. J. One-Pot Synthesis of New-Phase AgInSe2 Nanorods. *J. Am. Chem. Soc.* **2006**, *128* (22), 7118–7119. https://doi.org/10.1021/ja060543u.
(43) Cottingham, P.; Brutchey, R. L. On the Crystal Structure of Colloidally Prepared CsPbBr3 Quantum Dots. *Chem. Commun.* **2016**, *52* (30), 5246–5249. https://doi.org/10.1039/C6CC01088A.
(44) Rabuffetti, F. A.; Brutchey, R. L. Structural Evolution of BaTiO3 Nanocrystals Synthesized at Room Temperature. *J. Am. Chem. Soc.* **2012**, *134* (22), 9475–9487. https://doi.org/10.1021/ja303184w.
(45) Rabuffetti, F. A.; Culver, S. P.; Suescun, L.; Brutchey, R. L. Structural Disorder in AMoO4 (A = Ca, Sr, Ba) Scheelite Nanocrystals. *Inorg. Chem.* **2014**, *53* (2), 1056–1061. https://doi.org/10.1021/ic4025348.
(46) Krukau, A. V.; Vydrov, O. A.; Izmaylov, A. F.; Scuseria, G. E. Influence of the Exchange Screening Parameter on the Performance of Screened Hybrid Functionals. *J. Chem. Phys.* **2006**, *125* (22), 224106. https://doi.org/10.1063/1.2404663.
(47) Naumov, P.; Barkalov, O.; Mirhosseini, H.; Felser, C.; Medvedev, S. A. Atomic and Electronic Structures Evolution of the Narrow Band Gap Semiconductor Ag2Se under High Pressure. *J. Phys. Condens. Matter* **2016**, *28* (38), 385801. https://doi.org/10.1088/0953-8984/28/38/385801.
(48) Das, V. D.; Karunakaran, D. Variations of Energy Gap, Resistivity, and Temperature Coefficient of Resistivity in Annealed \ensuremath{\beta}-${\mathrm{Ag}}_{2}$Se Thin Films. *Phys. Rev. B* **1989**, *39* (15), 10872–10878. https://doi.org/10.1103/PhysRevB.39.10872.